# Nanoscale

Accepted Manuscript


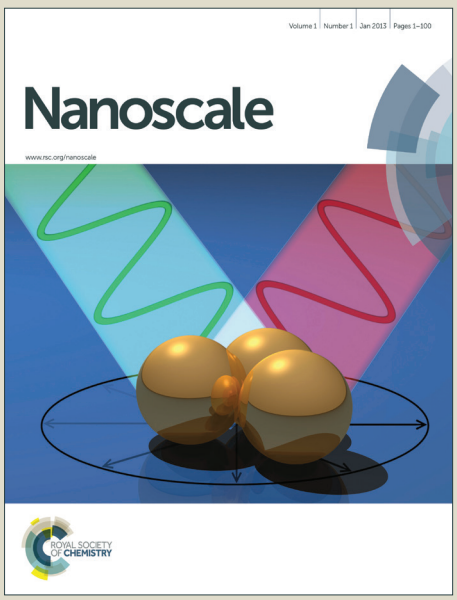





ROYAL SOCIETY OF CHEMISTRY

www.rsc.org/nanoscale

Nanoscale

MINIREVIEW

# Vanadium-based nanostructure materials for secondary lithium battery applications

Received 00th January 20xx,
Accepted 00th January 20xx

DOI: 10.1039/x0xx00000x

www.rsc.org/

Huiteng Tan,[b] Xianhong Rui,*[abc] Wenping Sun,[b] Qingyu Yan*[bc] and Tuti Mariana Lim*[d]

Vanadium-based materials, such as $V_2O_5$, $LiV_3O_8$, $VO_2$(B) and $Li_3V_2(PO_4)_3$ are compounds that share the characteristic of intercalation chemistry. Their layered or open frameworks allow facile ion movement through the interspaces, making them promising cathodes for LIB applications. To bypass the bottlenecks occurred in electrochemical performances of vanadium-based cathodes that derived from their intrinsic low electrical conductivity and ion diffusion coefficient, nano-engineering strategy is implemented to "create" the newly emerged properties that are unattainable at their bulk solids level. Integrating this concept in vanadium-based cathodes represents a promising way to circumvent the aforementioned problems as nanostructuring offer potential improvement in electrochemical performances by providing them shorter mass transport distance, higher electrode/electrolyte contact interfaces, and better accommodation of strain upon lithium uptake/release. The significance of nanoscopic architectures have been exemplified in literatures, showing that the prospect of developing vanadium-based nanostructures is an exciting direction to be explored. In this review, we will be casting light on recent advances in the synthesis of nanostructured vanadium-based cathodes. Furthermore, efficient strategies such as hybridization with foreign matrices and elemental doping are introduced as a possible way to boost higher level of their electrochemical performances (e.g., rate capability, cycling stability). Finally, some suggestions associated with the perspective for future development of vanadium-based cathodes are made to provide insight into their commercialization.

## Introduction

The energy industry is in the midst of a transformation since the alarm bells start ringing over the environmental pollution caused by the combustion of fossil fuel. As an alternative sustainable energy system, rechargeable lithium ion batteries (LIBs) are leading renewable energy storage technology in current market. A typical LIB system involves the release of lithium ions from the lithiated cathodes and migrate across the separator to insert into the anodes during charge and the electrochemical reaction happens reversely during discharge.[1-3] Traditional anode materials (e.g., graphite, oxides, and sulfides) generally possess higher theoretical specific capacity as compared to cathode materials (e.g., $LiCoO_2$, $LiFePO_4$, and $Li_4Ti_5O_{12}$) and hence, a breakthrough in LIBs lies in the successful research of advanced cathode materials as they are the primary limiting factor that hinders LIBs from realizing their full potential in term of energy density. The state-of-the-art cathode materials focus on intercalation compounds with a layered or open framework to allow facile Li ion movement. Amongst the cathodes that share the characteristic of intercalation chemistry, vanadium-based materials such as $V_2O_5$, $LiV_3O_8$, $VO_2$(B) and $Li_3V_2(PO_4)_3$ hold great promise as they possess desirable structure based on the arrangement of $VO_6$ octahedra in corner or edge sharing for reversible lithium uptake/release and a number of electrochemically accessible oxidation states (+5, +4, and +3) for electron transition. However, the progress of these vanadium-based cathodes in commercial application poses challenges arising from their sluggish lithium ion diffusion and low electrical conductivity.

Nanotechnology is regarded as a means of pushing the frontier of materials science. With its advances, a new wave of research is brought about in battery chemistry as the properties of nanomaterials are unattainable at their bulk solids level. It is generally accepted that the transport kinetics of a LIB is governed by the lithium ion diffusion time $t$, according to the following equation: $t = L^2/D$, where $L$ is the diffusion length and $D$ is the diffusion constant.[4] In other words, the ion and electron transport distance can be tremendously shortened after down-sizing the electrode materials to nano-regime.[4] Another advantage derived from nanotechnology is that the tailored electrode materials are endowed with higher surface area to allow high lithium-ion flux across the interfaces.[4] Implementing this concept in vanadium-based cathodes represents a promising way to circumvent the aforementioned problems as nanostructuring offers potential improvement in electrochemical performances by providing them shorter mass transport distance, higher electrode/electrolyte

[a] School of Energy and Environment, Anhui University of Technology, Maanshan, Anhui, 243002, China. E-mail: xhrui@outlook.com
[b] School of Materials Science and Engineering, Nanyang Technological University, 639798, Singapore. E-mail: alexyan@ntu.edu.sg
[c] Energy Research Institute, Nanyang Technological University, 637459, Singapore
[d] School of Civil and Environmental Engineering, Nanyang Technological University, 639798, Singapore. E-mail: tmlim@ntu.edu.sg

contact interfaces, and better accommodation of strain upon lithium uptake/release. The significance of nanoscopic architectures have been exemplified in literatures, showing that the prospect of developing vanadium-based nanostructures is an exciting direction to be explored.[5-7]

Following the previous reviews on some vanadium-based materials in primary lithium batteries[8, 9] and vanadium redox flow batteries,[10] this mini review will summarize some recent development of vanadium-based (i.e., $V_2O_5$, $LiV_3O_8$, $VO_2$(B) and $Li_3V_2(PO_4)_3$ covering the vanadium oxidation states from +5 to +3) nanostructures as cathodes in LIBs (Fig. 1), highlighting crystal structures, electrochemical lithium charge/discharge mechanisms, and the electrode engineering strategies employed in tailoring the phase, morphology, and size based on their classification as zero-dimensional (0D), one dimensional (1D), two-dimensional (2D) and three-dimensional (3D). Furthermore, several approaches such as hybridization and elemental doping will be introduced to explain their contributions towards the enhancement in electrochemical performances of LIBs. Lastly, future prospect for possible research trends in electrode design and architecture will be discussed herein.

## $V_2O_5$ nanostructures for LIBs

Orthorhombic $V_2O_5$ (space group: *Pmmn*; $a$ = 11.512 Å, $b$ = 3.564 Å, $c$ = 4.368 Å) shows layered structural characteristic and its square-pyramidal coordination polyhedron is arranged in an up-up-down-down sequence by sharing edges and corners.[11] The intercalation mechanism of Li in $V_2O_5$ can be generalized as: $V_2O_5 + xLi^+ + xe^- \rightarrow Li_xV_2O_5$, in which a series of phase transition is associated with the content of inserted Li. Trace amount of Li intercalation results in α-$Li_xV_2O_5$ ($x < 0.01$) which is subsequently transformed into ε-$Li_xV_2O_5$ ($0.35 < x < 0.7$) after further lithiation. Insertion of exactly one Li leads to the formation of δ-phase $Li_xV_2O_5$ but more than that converts it to an irreversible form of γ-$Li_xV_2O_5$ ($1 < x < 2$). At a maximum Li insertion, irreversible transformation of γ-$Li_xV_2O_5$ to rock-salt type ω-$Li_xV_2O_5$ ($2 < x < 3$) occurs.

Narrowing the particle size of $V_2O_5$ from micron- to nano-scale has made the merits of nanostructing to be more prominent. Previous works done on synthesizing $V_2O_5$ nanoparticles have been accomplished by physical approaches, such as sputtering,[12-13] thermal evaporation[14] and spray deposition[15-16] to construct a thin film electrode. However, nanoparticles have great tendency to agglomerate and lose their active surface towards lithium associated reactions. Thus, great effort has been made on stabilize them within a foreign matrices or transforming into a more sustainable structure. For instances, nanocrystalline $V_2O_5$ nanoparticles were entrapped in a 3D open framework to exert some kind of confinement to the mobility of the nanoparticles, which will be discussed in the following section. Similar principle is also employed as the 3D matrix was substituted with microporous filtration membrane.[17] Both of them minimize a great deal of capacity loss associated with the agglomeration of nanoparticles.

1D $V_2O_5$ can be categorized into nanorods,[18-19] nanoribbons,[20] and nanowires[21-23] depending on different aspect ratio. The electron transport process is much more efficient along the micro-scale axis of 1D $V_2O_5$, making it viable candidates for battery applications. In this regard, $V_2O_5$ with several centimeters long and 80-120 nm in diameter were successfully synthesized by Zhai et al.[22] using a simple hydrothermal method. The as-prepared nanowires exhibit a specific capacity of 175 mA h $g^{-1}$ at the current density of 50 mA $g^{-1}$ during the 20$^{th}$ cycle. A method that combined the sol-gel chemistry with electrospinning was developed by Yu and co-workers[23] to precisely control over the dimension of 1D $V_2O_5$ without the aid of sacrificial template. On the other hand, the annealing process carbonized/evaporated the soft template, rendering the 1-D structure highly porous. This morphological feature facilitates the charge transport without destructing the interconnected electron transfer pathway, giving rise to a specific capacity of 370 mA h $g^{-1}$ at 800 mA $g^{-1}$ with slightly capacity fading.

In recent years, 2D materials, including nanosheets[24-25] and entanglement network of nanobelts[26-27] have been actively pursued as they offer sufficiently high surface area for electrochemical reaction and their ultrathin thickness is beneficial for enhanced transport kinetics. In a liquid exfoliation method developed by Rui *et al.*,[24] they made use of small organic molecules (formamide) as delaminating agent to intercalate into the crystal lattice of bulk $V_2O_5$. Then, ultrathin $V_2O_5$ nanosheets can be nicely exfoliated by a simple mechanical shaking, as depicted in Fig. 2a. The X-ray diffraction pattern (XRD) shows the success preparation of the {001} orientated $V_2O_5$ nanosheets (Fig. 2b). The transmission electron microscopy (TEM) exposure reveals that the $V_2O_5$ nanosheets have lateral dimensions of 100-400 nm which are dispersed homogeneously in the solution over several weeks (Fig. 2c). From the SAED pattern as shown in Fig. 2d, a highly (001)-oriented diffraction spots can be clearly observed. In addition, atomic force microscopic (AFM) measurement illustrates that the thickness of a single nanosheet is about 2.1-3.8 nm. The initial charge-discharge voltage profile shows three typical plateaus corresponding to the phase transitions of $V_2O_5 \rightarrow Li_{0.5}V_2O_5 \rightarrow Li_{1.0}V_2O_5 \rightarrow Li_{2.0}V_2O_5$ at around 3.4, 3.2 and 2.3 V, respectively. In contrast to the rapid capacity fading of the bulk sample, the nanosheet can still deliver specific capacity of 274 mA h $g^{-1}$ after 50 cycles, corresponding to 93.8% of capacity retention. Moreover, the nanosheets also exhibit an excellent rate performance, in which 2$^{nd}$-cycle discharge capacities of 266, 251, 233, 192, 156, and 137 mA h $g^{-1}$ can be reached at 1, 3, 5, 10, 20, and 30 C, respectively (Fig. 2e). As illustrated in the Ragone plot (Fig. 2f), the $V_2O_5$ nanosheet electrode shows impressive high-power and high-energy performance as compared to other energy storage devices, in which a gravimetric energy of 158 W h $kg^{-1}$ at a power rate of 20 kW $kg^{-1}$ is obtained. The enhanced performances were mainly derived from the unique 2D structure of $V_2O_5$, giving them higher surface area, shorter diffusion paths for charge carrier and better strain relaxation upon lithium intercalation/de-intercalation.

On the other hand, the concept of using entanglement network of 1D $V_2O_5$ as binder-free electrode was practically illustrated by Rui and co-workers.[26] The hydrated $V_2O_5$ (HVO) nanobelts were synthesized via a hydrothermal method. The microscopic images of the HVO show that the HVO possesses nanobelt morphology with length of 100-400 mm (Fig. 3a and b), width of 20-600 nm (Fig. 3c), and thickness of 10 nm (Fig. 3d). As depicted in Fig. 3e, the HVO nanobelts are highly crystalline with its long micron-axis is orientated along the [010] direction. Successful attempt in

fabricating the HVO into bulky paper has been demonstrated as Fig. 3f, in which a flexible electrode is robust upon bending. The absence of polymeric binder (e.g., PVDF) neither disrupts the electrode integrity nor its flexibility. The electrochemical charge and discharge tests reveal that the HVO bulky paper electrode could still consistently maintain almost 100% Coulombic efficiency during the 20 cycles despite of slight drop in discharge capacity. Moreover, the electrode can deliver discharge capacities of 283, 241, 212, 194, 183, and 163 mA h $g^{-1}$ during the 2$^{nd}$ cycle at current rates of 0.34, 0.68, 1.7, 2.7, 3.4 and 6.8 C, respectively, which outperform the traditionally PVDF-added HVO cathodes. Electrochemical impedance measurement demonstrates the benefit of excluding the electro-inert binder, in which the smaller radius of semi-circle of the binder-free HVO electrode clearly indicates its lower charge transfer resistance as compared to the PVDF-added HVO cathodes. The enhancement is closely associated with the intertwined nanobelt network that provides hierarchical porous channels for better ion penetration and the binder-free fabrication that improves the electronic conductivity.

The 3D robust framework is adopted to provide free penetration of ions, allowing every single active site to be easily accessible. On the other hand, the interconnected framework also constructs a continuous highway for better electron transport. Besides, the construction of secondary structures that self-assembled by nanoparticles under polyol-mediated environment, in particularly hollow sphere has been demonstrated to be able to allow excellent charge transport while be able to prevent nanoparticles from aggregating into large clusters. In literature, $V_2O_5$ thin film that composed of interconnected porous network was successfully achieved using a simple electrostatic spray pyrolysis method.[28] Its excellent rate performance is derived from the porous framework to enable fast lithium diffusion, giving rise to retain specific capacity of 87 mAh $g^{-1}$ at 56 C (8232 mA $g^{-1}$). Additionally, nanoscale $V_2O_5$ building blocks with different morphologies are also strategically assembled into 3D structures.[29-31] For instances, Pan *et al.*[29] has developed facile solvothermal method to obtain hierarchical $V_2O_5$ hollow microflower. The as-prepared sample exhibits good capacity retention in the cycling test with only showing 0.27% capacity loss in each cycle in a voltage window of 2.0-4.0 V.

The presence of graphitic support proved to be essential in addressing the electronic conductivity and structural stability of $V_2O_5$, in which the carbonaceous materials can be categorized into 1D CNTs,[32-35] 2D graphenes,[36-38] *etc*. In this regard, Rui *et al.*[39] hybrized the reduced graphene oxide (rGO) with the highly porous $V_2O_5$ spheres (denoted as $V_2O_5$/rGO) using a simple solvothermal method, as shown in Fig. 4a. Uniform attachment of rGO onto the surface of $V_2O_5$ sphere is driven by the heterogeneous nucleation and precipitation of vanadium on rGO before sintering. After the annealing process, the $V_2O_5$ nanoparticles tend to assemble into hollow sphere to reduce the total surface energy. Before sintering, $V_2O_5$ with particle size of 10-50 nm are uniformly attached onto the surface of rGO (Fig. 4b). Interestingly, they turn into hollow sphere with diameters of 200-800 nm (Fig. 4c and d) and are constructed by interconnected small grains of 50 nm (Fig. 4e). The weight percentage of rGO is about 46 wt%. Such hybrid exhibits a relatively low capacity fading rate at 90 mA $g^{-1}$, in which about 0.30% of capacity is degraded per cycle over the total 50 cycles. Rate performance test displays 211, 200, 184, 175, 167, 127 and 102 mA h $g^{-1}$during the 2$^{nd}$cycle at 190 (0.65 C), 380 (1.3 C), 950 (3.2 C), 1520 (5.2 C), 1900 (6.5 C), 3800 (13 C) and 5700 mA $g^{-1}$ (19 C), respectively (Fig. 4f). In addition, even at current density as high as 5700 mA $g^{-1}$ (19 C), the electrode can still achieve 93 mA h $g^{-1}$ after 200 cycles (Fig. 4g). These enhancements can be explained by having the conductive support and unique hollow structures. The presence of rGO facilitates the charge transfer between the active materials and the current collector. On the other hand, the porous and hollow architectures provide good shorter lithium diffusion path by giving better electrolyte penetration to the active materials.

The doping for $V_2O_5$ has been introduced to replace the V with cations ($Ag^+$, $Cu^{2+}$, $Cr^{3+}$, $Mn^{2+}$, $Sn^{2+}$, *etc*.)[40-44] to alter the valence state of V for high electronic conductivity and better lithium ion diffusion across the crystal lattice of $V_2O_5$. Yu *et al.*[41] has synthesized hierarchical Cu-doped $V_2O_5$ (e.g., $Cu_{0.02}V_{1.98}O_5$) flowers that self-assembled from $V_2O_5$ nanobelts using a simple hydrothermal method. As illustrated in the formation mechanism of the Cu-doped $V_2O_5$ shown in Fig. 5a, it started from preferential growth of nanoparticles into nanobelts followed by the self-assembled of flower-like secondary structures without any aid from surfactant. From the SEM images, the 10 μm flower-like porous network (Fig. 5b) is constructed by nanobelts with lateral dimension of ~100 nm (Fig. 5c). It is also found that the Cu-doped $V_2O_5$ nanobelts are highly crystalline with a long axis along the [010] direction (Fig. 5d and e). Comparing the CV curves of pure $V_2O_5$ (Fig. 5f) and Cu-doped $V_2O_5$ nanobelts (Fig. 5g), the doped sample shows better symmetry. Explanation on such an observation is that the structural changes are suppressed after the Cu doping, giving rise to better reversibility and stability. On the other hand, the electrochemical performances of the Cu-doped $V_2O_5$ surpass the un-doped sample. For examples, cycling retention for the Cu-doped $V_2O_5$ ($V_2O_5$-2, $Cu_{0.02}V_{1.98}O_5$) and un-doped samples are 85% and 69%, respectively during the 50$^{th}$ cycle (Fig. 5h). The Cu-doped $V_2O_5$ also show promising results in rate performance, in which 2$^{nd}$ cycle capacities of 229, 197, 182, 126 and 97 mA h $g^{-1}$ can be achieved at 1.0, 3.0, 5.0, 10 and 20.0 C, respectively (Fig. 5i). The authors attributed that the Cu-doping has decreased the charge transfer resistance by improving the lithium diffusion kinetics of the Faradic reactions, giving rise to better cycling performance and rate capability.

Furthermore, the structural characteristics of $V_2O_5$ enable the intercalation of cations or small molecules (other than Li) at the interlayer position between square pyramidal $VO_5$ layers.[45-47] With such an interesting property, it has inspired researches to tune the lithium ion diffusion rate and collapse of lattice structure through modification of interlayer spacing of $V_2O_5$. In literature, successful attempt has been made on controlling the hydration level and sodium content of $Na_xV_2O_5{\cdot}nH_2O$ using a chimie douse strategy.[45] Electrochemical assessment of the hydrated sodium vanadium oxides reveals that the capacities increase with the decreasing water content, in which specific capacities of 170 and 300 mA h $g^{-1}$ are achieved by $Na_{0.12}V_2O_5{\cdot}0.23H_2O$ and $Na_{0.32}V_2O_5{\cdot}0.01H_2O$, respectively, at discharge rate of C/20.

## $LiV_3O_8$ nanostructures for LIBs

Layered trivanadate, $LiV_3O_8$ belong to a monoclinic system (space group: $P2_1/m$, a = 6.680 Å, b = 3.596 Å, c = 12.024 Å), in which the immobile $Li^+$ ions reside at the octahedral coordination of the $[V_3O_8]$ interlayer space.[48] It is interesting that the empty tetrahedral sites of $LiV_3O_8$ can be continuously occupied by incoming $Li^+$ ions during discharging without causing irreversible distortion of the crystal structure, leading to the formation of non-stoichiometric $Li_{1+x}V_3O_8$ ($0 < x < 3$) that is able to accommodate up to 3 $Li^+$ per formula unit and yields theoretical capacity of 280 mA h $g^{-1}$.[49]

The lithium insertion process of $Li_{1+x}V_3O_8$ involves several phase transition steps. Single-phase transitions occur at the potentials of 3.5, 2.8, 2.7, and 2.3−2.4 V, in which $Li^+$ fills the tetrahedral sites. On the other hand, $Li^+$ fills the octahedral sites ($Li_3V_3O_8$ to $Li_4V_3O_8$) *via* a two-phase transition at potential of 2.5 V.[50-53] At a relatively low potential of 2.3 V, the slow kinetic intercalation step is regarded as the origin of capacity fading due to reactions between the $Li_4V_3O_8$ and electrolyte that lead to passive film formation or the dissolution of the active species.[54]

To have a more precise control over the homogeneity and particle size of $LiV_3O_8$, solid-state reaction and traditional high-temperature sintering method have been substituted with alternative approaches, such as sol-gel methods,[51, 55-57] hydrothermal reaction,[58-59] microwave-assisted reaction,[60-61] spray pyrolysis,[62] topotactic synthesis,[63] *etc*. Xu *et al.*[63] topotactically synthesized ultralong $LiV_3O_8$ nanowires from $HV_3O_8$ precursor. The lithium substitution process is allowed owing to their similarity in layered crystal structure. Fig. 6a-c show the morphology and microstructure of the as-synthesized $LiV_3O_8$. The 1D morphology is retained after calcinations at 450 °C. Fig. 6d depicts the characteristic redox peaks of $LiV_3O_8$ in the voltage range of 4.0 – 1.5 V, which is in accordance with the charge/discharge curves shown in Fig. 6e. It is found that the $LiV_3O_8$ electrode calcined at 450 °C achieves the best performances in rate capability and cycling tests. As demonstrated in Fig. 6f, discharge capacities of 279, 269, 253, 237, 222, 211 and 196 mA h $g^{-1}$ at current densities of 50, 100, 200, 300, 400, 500 and 600 mA $g^{-1}$, respectively, are achieved by the $LiV_3O_8$ electrode calcined at 450 °C. Moreover, it also performs well at high current densities, in which discharge capacities of 160 and 120 mA h $g^{-1}$ are retained after 400 and 600 cycles, respectively.

Other than tuning the particle size and morphology of $LiV_3O_8$, several approaches have been devised to improve the electrochemical performances of $LiV_3O_8$ by control of crystallinity[64-65], tailoring of interlayer spacing,[59, 66] cations substitution,[67-69] doping,[70-71] and surface coating.[72-73] It is still a controversial issue concerning the influences of degree crystallinity on the performances of $LiV_3O_8$. Early reports showed that the better electrochemical performances of low crystallinity $LiV_3O_8$ were due to the fact that the presence of bound water molecules enlarged the lattice spacing of $LiV_3O_8$, increasing the mobility $Li^+$ ion across the 2D diffusion pathway.[64-65] However, in a latter study reported by Pan *et al.*,[51] they proved that the disordered atom arrangement of low crystallinity $LiV_3O_8$ may interfere the $Li^+$ ion diffusion across the host materials. Applying similar concept of previous report that controlled the crystallinity of $LiV_3O_8$ to increase the interlayer spacing, Yu *et al.*[66] synthesized $LiV_3O_8$ and deliberately intercalated water molecules into its host lattice. The hydrated $LiV_3O_8$ (250 mA h $g^{-1}$) delivers higher specific capacity than the crystalline or dehydrated $LiV_3O_8$ (175 mA h $g^{-1}$) and shows better cycling stability. Cation substitution has been employed to improve the crystal lattice stability during the rearrangement of oxygen packing upon phase transition. For example, Ni was doped to improve the cycling stability of the pristine $LiV_3O_8$. Specific capacity of 251 mA h $g^{-1}$ is retained after 30 cycles at 0.5 C by the Ni doped $LiV_3O_8$, surpassing the undoped sample.

## $VO_2$(B) nanostructures for LIBs

$VO_2$ exists in several polymorphic forms, such as rutile $VO_2$(R), monoclinically distorted rutile $VO_2$(M), tetragonal $VO_2$(A), and monoclinic $VO_2$(B).[74] In particular, the metastable $VO_2$(B) offers layered structural characteristic, in which the adjacent $VO_5$ square pyramids are connected at basal edges with the vanadyl groups arranging in a manner of alternate up and down.[75] Typical plateaus observed at 2.5 V during discharge and 2.6 V during charge in the CV measurement represent the reversible insertion and withdrawal of lithium into the layered structure of $VO_2$(B), giving rise to theoretical capacity of 161 mA h $g^{-1}$. Its general expression is shown as follows:[76]

$$VO_2 + 0.5Li^+ + 0.5e^- \rightarrow Li_{0.5}VO_2$$

Nanocrystalline $VO_2$(B) has been documented to be synthesized by reduction of $V_2O_5$ powder using borohydride solution.[77-78] By using this method, the particle size of $VO_2$(B) can be reduced to approximately 100 nm. In the literature, $VO_2$(B) has been mostly reported as 1D nanostructures.[74, 78-80] Although good lithium storage properties have been improved using 1D nanostructures, their rate capabilities are still far from being satisfactory. Hence, carbon coating[81-83] and hybridizing with carbonaceous materials[83-88] are implemented to improve the electronic conductivity of $VO_2$(B). In this regard, carbon coated $VO_2$(B) was synthesized by Rui *et al.*[81] using a hydrothermal method, in which the in-situ growth of amorphous carbon that is derived from sucrose is intimately attached on the surface of $VO_2$(B). The belt-like morphology of the $VO_2$(B)@C(6.6 wt%) sample is shown in Fig. 7a, which possesses a width of ~120-130 nm (Fig. 7b) and a thickness of ~25 nm (Fig. 7c). From the HRTEM exposure shown in Fig. 7d, the thickness of the amorphous carbon layer is approximately 4.3 nm. The thickness of the carbon layer is controllable by adjusting the concentration of sucrose. Having a relatively thick carbon layer may block the lithium diffusion pathway although the electrical conductivity and the structural strain accommodation can be improved substantially. Hence, only optimum thickness of carbon layer renders the electrode excellent electrochemical performances. The voltage profiles (Fig. 7e) and cycling performances (Fig. 7f) of the $VO_2$(B)@C samples are similar. However, the $VO_2$(B)@C(6.6 wt.%) exhibits the best rate capability, in which discharge capacities of 157, 155, 146 and 136 mA h $g^{-1}$ can be achieved during the 2nd cycle at current densities of 200 (1.2 C), 500 (3.1 C), 800 (5.0 C) and 1000 mA $g^{-1}$ (6.2 C), respectively, by striking a balance between the electronic conductivity and lithium ion diffusion efficiency (Fig. 6g). As revealed by the electrochemical impedance spectrum (EIS) measurements, the $VO_2$(B)@C(6.6 wt%) cathode shows a semi-circle with the smallest radius among other samples, indicating its

faster kinetics of the Faradic reactions by having the lowest charge-transfer resistance.

As an alternative to further improve the electrochemical performance, research works have been done on incorporating functional nanostructures to mitigate the structural stability problem during lithiation/de-lithiation. In particular, Mai and co-workers[89] has successfully demonstrated the idea of using nanoscroll buffered hybrid nanostructural $VO_2$ composed of nanobelts and nanowires using a hydrothermal-driven splitting and self-rolled method. The unique structural features of the buffer layer offer facile relaxation strain to accommodate the volume variation during electrochemical reaction, enabling them to retain 82% of its initial capacity after 1000 cycles at 9 C (1,000 mA $g^{-1}$). Substantial efforts have been dedicated to the synthesis of $VO_2$(B) in 3D nanostructures, including sacrificial-template or template-free approaches.[90-92] It is believed that the radially protruding $VO_2$(B) nanostructures that assembled into a sphere have better accommodation to expansion/shrinkage and be able to suppress self-aggregation.

## $Li_3V_2(PO_4)_3$ nanostructures for LIBs

$Li_3V_2(PO_4)_3$ (LVP) exists in two different polymorphic forms which are rhombohedral (or so-called NASICON) and monoclinic phases. The NASICON framework of LVP (space group: $R\bar{3}c$; $a$ = 8.316 Å, and $c$ = 22.484 Å) is constructed by interconnected $VO_6$ octahedra and $PO_4$ tetrahedra through their vertices in the [001] direction to form the $[V_2(PO_4)_3]$ lantern, where the lithium is located in a 4-fold coordinated interstitial site.[93] As compared to the rhombohedral LVP, monoclinic LVP (space group: $P2_1/n$, $a$ = 8.605 Å, $b$ = 8.591 Å, $c$ = 12.038 Å, and $\beta$ = 90.600) is more thermodynamically stable. Its $VO_6$ octahedra and $PO_4$ tetrahedra are connected through oxygen vertexes, where three crystallographic interstitial voids are available for the occupancy of lithium.[94]

The structural differences render them to undergo distinct electrochemical reaction. Rhombohedral LVP is reported to undergo two-phase transition between the compositions of $Li_3V_2(PO_4)_3$ and $Li_1V_2(PO_4)_3$ (3.7 V), involving the $V^{3+}/V^{4+}$redox couple. The symmetry of the monoclinic LVP allows three lithium that accommodated within the $[V_2(PO_4)_3]$ lanterns to be mobile enough to participate in the electrochemical reaction (voltage range of 3.0-4.8 V). During the de-lithiation step, the lithium content of $Li_xV_2(PO_4)_3$ varies from $x$ = 3.0, 2.5, 2.0, 1.0 and 0 through a complex series of phase transition, corresponding to the following equations:

$$Li_3V_2^{3+}(PO_4)_3 - 0.5Li^+ - 0.5e^- \rightarrow Li_{2.5}V^{3+}V_{0.5}^{4+}(PO_4)_3$$

$$Li_{2.5}V^{3+}V_{0.5}^{4+}(PO_4)_3 - 0.5Li^+ - 0.5e^- \rightarrow Li_2V^{3+}V^{4+}(PO_4)_3$$

$$Li_2V^{3+}V^{4+}(PO_4)_3 - Li^+ - e^- \rightarrow LiV_2^{4+}(PO_4)_3$$

$$LiV_2^{4+}(PO_4)_3 - Li^+ - e^- \rightarrow V_2^{4.5+}(PO_4)_3$$

The working potential of LVP is relatively higher over other vanadium-based cathodes, in which 3 lithium de-intercalation reaction within voltage range of 3.0–4.8 V is achievable, giving rise to a theoretical capacity of 197 mA h $g^{-1}$. Based on a systematic study reported by Rui and co-workers,[95] the authors found that the correlation between the voltage state of charge/discharge and chemical diffusion coefficient of lithium ion in LVP in the potential range of 3.0 - 4.8 did not change significant in spite of using different techniques (CV, GITT, and EIS). As illustrated in Fig. 8, all these three measurements showed a "W" shape curve which is indicative of the characteristics of insertion-host materials. Besides, the chemical diffusion coefficient derived from the aforementioned techniques is in the range of $10^{-19}$ – $10^{-10}$ $cm^2$ $s^{-1}$, indicating that LVP is a promising candidate for high-rate battery applications.

In literature, significant improvement has been observed when LVP bulk materials are engineered to reach nano-level. The most commonly used methods are traditional solid-state reaction[96-98], sol-gel reaction[99-101], hydrothermal method[102-104], spray pyrolysis, and other methods[105-107]. As compared to the aforementioned methods, sol-gel and hydrothermal reactions are more favorable as they can produce LVP nanoparticles with good homogeneity, uniform morphology and controllable particle size, giving rise to higher charge/discharge rate. For instances, Liu *et al.*[104] reported that uniform LVP nanorods with a diameter of ~60 nm and a length of 0.5-1.0 µm can be synthesized using a hydrothermal method. The LVP nanorods show good rate performance, in which specific capacities of 141.6, 136.1, 134.6, 124.8 and 101.1 mA h $g^{-1}$ can be delivered at the 0.5, 1, 2, 5 and 10 C, respectively, in the voltage range of 3.0-4.6 V. LVP with particle size in the range of 200-500 nm has also been successfully synthesized using a sol-gel method.[108] It shows specific capacity of about 100 mA h $g^{-1}$ at 1 C after 80 cycles and close to 100% Coulumbic efficiency during the cycling test. To meet the burgeoning demand for the performance of cathode materials, LVP nanomaterials are further modified to overcome their kinetic limitations. Several approaches will be covered in this review: (1) carbon coating;[109-111] (2) other additive coating;[112-114] and (3) doping. Carbonaceous materials (graphene and amorphous carbon) and conductive additives (Ag, Nb, glassy lithium phosphate, $SiO_2$) are coated onto the surface of LVP for the same reasons which act as the conductive matrices and buffer layers to restrain structural deformation. Non-conductive additive (MgO and $SiO_2$) are used to stabilize the structure of LVP from dissolution and decreases the interface charge transfer resistance. The doping system is complicated, in which the dopants can be supervalent cations ($Na^+$, $Ca^{2+}$, $Co^{2+}$, $Mn^{2+}$, $Mg^{2+}$, $Fe^{3+}$, *etc.*),[115-120] and anions ($F^-$ and $Cl^-$).[121-122] It is found that this approach can improve the intrinsic electronic conductivity and lithium ion diffusion of LVP.

In an interesting report, the influences of different carbon sources on the electrochemical performances of LVP electrodes were investigated.[109] Here, micron-size LVP were synthesized by a carbon thermal reduction process using citric acid, glucose, PVDF and starch as both reduction agents and carbon coating sources. Four as-prepared samples show good rate capability and display almost no capacity fading after 100 cycles in the voltage range of 3.0-4.3 V. These good performances could be attributed to the presence of uniform carbon layer to reduce the resistance and improve their electronic conductivity. On the other hand, Rui *et al.*[110] has demonstrated the possibility of coupling the ultrafine LVP that embedded in nanoporous carbon matrix with reduced graphene oxide (rGO), so-called LVP-NC@NPCM@rGO, to build a binder-free cathode for LIBs. The LVP-NC@NPCM@rGO was synthesized using sol-gel chemistry and followed by a thermal

annealing process. 20-80 nm quasi-spherical nanoparticles are uniformly attached on the surface of rGO and nanocrystals with size of 5-8 nm are embedded in a single cluster. The LVP-NC@NPCM@rGO shows excellent rate capability, in which discharge capacities of 168, 164, 160, 154, 145, 136, 126 and 109 mA h $g^{-1}$ can be achieved during the 2$^{nd}$ cycle at current densities of 197 (1 C), 394 (2 C), 591 (3 C), 985 (5 C), 1970 (10 C), 2955 (15 C), 3940 (20 C) and 5910 mA $g^{-1}$ (30 C), respectively, between 3.0 and 4.3 V. Impressively, in the wider voltage window of 3.0-4.8 V, the LVP-NC@NPCM@rGO can still exhibit a superior high-C-rate performance, e.g., 109 mA h $g^{-1}$ at 5910 mA $g^{-1}$ (30 C), and even delivers specific capacity of 91 mA h $g^{-1}$ after cycling for 1000 cycles at 30 C. Besides the contribution of nano-sizing, electrochemical improvement of the LVP-NC@NPCM@rGO can be attributed to the following aspects: (1) nanoporous carbon matrix facilitates fast $Li^+$ and $e^-$ transport across the active material/electrolyte interfaces and cushion the structural deformation of the LVP nanocrystals; (2) highly conductive rGO network provides better charge transfer between the active materials and current collector; (3) binder-free fabrication avoids the electro-inert species and allows better electrolyte permeation.

## Conclusions and Perspectives

In summary, this mini review highlighted recent advances in design and fabrication of nanostructured vanadium-based electrodes (i.e., $V_2O_5$, $VO_2$(B), $Li_3V_2(PO_4)_3$ and $LiV_3O_8$) for LIB applications. It is found that the intrinsic disadvantages of vanadium-based cathodes have been alleviated by exploiting their newly emerged properties that tailored by naonstructuring. Furthermore, the concept of hybridization with foreign matrices (conductive and non-conductive substrates such as carbonaceous materials, metals, metal oxides) and elemental doping have brought about further improvement to the existing single-phase vanadium-based cathodes. Additionally, significant advances have also been achieved in electrode fabrication process, making the electrodes more flexible, efficient, and accessible to electrolyte.

Although the aforementioned concepts have experimentally demonstrated their feasibilities to be electrochemically lithiated/delithiated, there still remains grand challenges to directly put them into practice. So far, almost all of methodologies for the fabrication of nanoarchitectured vanadium-based electrodes are still stuck in laboratory scale and far from meeting the specifications of industrial standards. Synthesizing the desired vanadium-based nanoarchitectures with high capacity and high rate performance is a significant step toward the practical applications. Another concern is that vanadium oxides and some salts of vanadium have moderate toxicity. Furthermore, despite nanostructures with high surface-to-volume ratios can facilitate efficient $Li^+$ transfer between the electrolyte and the active materials to achieve high-power performance, irreversible capacity caused by formation of passivation layers, or uncontrolled reactions, is greater. Regarding vanadium oxide cathodes, it is easy to form some irreversible lithiated phases when they are deeply discharged, which will result in seriously capacity fading. On the other hand, vanadium oxide cathodes (e.g., $V_2O_5$ and $VO_2$(B)) are Li deficient and may be only suitable for non-rechargeable primary lithium batteries in practice.

Applications of nanostructured vanadium-based cathode materials in LIB technology are still in the stage of research and development. To realize a wide range of industrial applications, further work is required to achieve progress on green and large-scale production, LIB performances and electrochemical characteristics, design of new vanadium-based cathodes, and so on. The synthetic process of vanadium-based cathodes has to fulfil several requirements, such as simple, scalable for mass production, cheap, and environmental benign for the prospect of commercial applications. Hence, there is still room for improvement and optimizing the synthetic protocol to achieve this goal. Continue improvement on cycling stability and rate capability of vanadium-based cathodes with nanocrystallization, surface coating, element substitution, material processing, etc., is needed. For example, there is still great development space in tailoring the nanoarchitectures and morphologies to obtain more favourable lithium storage properties, and a promising direction is the introduction of more complex hierarchical 3D micro-/nanostructures with internal void/pore space, which can avoid some limitations of using simple one component nanostructures. Furthermore, it is also highly essential to study the fundamental issues associated with the electrochemical characteristics (e.g., the kinetics of electron/ion transport at the electrode/electrolyte interface) of nanostructuresd vanadium-based cathodes which is regarded as a key for further breakthrough in materials optimization. On the other hand, searching for new vanadium-based cathodes with special characteristics (e.g., stable crystal structure, high electrical conductivity, high working potential, etc.) is also expected to significantly enhance their practical use in LIB devices.

## Acknowledgements

Q. Yan gratefully acknowledges Singapore MOE AcRF Tier 1 grants RG2/13, and Singapore National Research Foundation under CREATE program: EMobility in Megacities. X. Rui gratefully acknowledges the program of the Leading Talent Team in Universities of Anhui Province, China, and the National Natural Science Foundation of China (No. 51376007).

## Notes and references

1. M. S. Whittingham, *Chem. Rev.*, 2004, 104, 4271-4301.
2. J. M. Tarascon and M. Armand, *Nature*, 2001, 414, 359-367.
3. X. Rui, H. Tan and Q. Yan, *Nanoscale*, 2014, 6, 9889-9924.
4. P. G. Bruce, B. Scrosati and J. M. Tarascon, *Angew. Chem. Int. Ed.*, 2008, 47, 2930-2946.
5. Q. Zhang, E. Uchaker, S. L. Candelaria and G. Cao, *Chem. Soc. Rev.*, 2013, 42, 3127-3171.

6. M. Wagemaker, W. J. H. Borghols and F. M. Mulder, *J. Am. Chem. Soc.*, 2007, 129, 4323-4327.
7. Y. Tang, X. Rui, Y. Zhang, T. M. Lim, Z. Dong, H. H. Hng, X. Chen, Q. Yan and Z. Chen, *J. Mater. Chem. A*, 2013, 1, 82-88.
8. K. J. Takeuchi, A. C. Marschilok and E. S. Takeuchi, in Vanadium: Chemistry, Biochemistry, Pharmacology and Practical Applications (Eds: A. S. Tracey, G. R. Willsky and E. S. Takeuchi), Taylor and Francis, New York, 2007, Ch. 13.
9. E. S. Takeuchi, K. J. Takeuchi and A. C. Marschilok, in Encyclopedia of Electrochemical Power Sources (Ed: G. Jürgen), Elsevier, Amsterdam, 2009, 100-110.
10. A. Parasuraman, T. M. Lim, C. Menictas and M. Skyllas-Kazacos, *Electrochim. Acta*, 2013, 101, 27-40.
11. R. Enjalbert and J. Galy, *Acta Crystallogr. Sect. C*, 1986, 42, 1467-1469.
12. N. Kumagai, H. Kitamoto, M. Baba, S. Durand-Vidal, D. Devilliers and H. Groult, *J Appl. Electrochem.*, 1998, 28, 41-48.
13. K. West, B. Zachau-Christiansen, S. V. Skaarup and F. W. Poulsen, *Solid State Ionics*, 1992, 57, 41-47.
14. M. D. Levi, Z. Lu and D. Aurbach, *J. Power Sources*, 2001, 97–98, 482-485.
15. S.-H. Ng, T. J. Patey, R. Buchel, F. Krumeich, J.-Z. Wang, H.-K. Liu, S. E. Pratsinis and P. Novak, *Phys. Chem. Chem. Phys.*, 2009, 11, 3748-3755.
16. Y.-T. Kim, S. Gopukumar, K.-B. Kim and B.-W. Cho, *J. Power Sources*, 2003, 117, 110-117.
17. C. J. Patrissi and C. R. Martin, *J. Electrochem. Soc.*, 1999, 146, 3176-3180.
18. A. Pan, J.-G. Zhang, Z. Nie, G. Cao, B. W. Arey, G. Li, S.-q. Liang and J. Liu, *J. Mater. Chem.*, 2010, 20, 9193-9199.
19. K. Takahashi, S. J. Limmer, Y. Wang and G. Cao, *J. Phys. Chem. B*, 2004, 108, 9795-9800.
20. C. K. Chan, H. Peng, R. D. Twesten, K. Jarausch, X. F. Zhang and Y. Cui, *Nano Lett.*, 2007, 7, 490-495.
21. L. Mai, L. Xu, C. Han, X. Xu, Y. Luo, S. Zhao and Y. Zhao, *Nano Lett.*, 2010, 10, 4750-4755.
22. T. Zhai, H. Liu, H. Li, X. Fang, M. Liao, L. Li, H. Zhou, Y. Koide, Y. Bando and D. Golberg, *Adv. Mater.*, 2010, 22, 2547-2552.
23. D. Yu, C. Chen, S. Xie, Y. Liu, K. Park, X. Zhou, Q. Zhang, J. Li and G. Cao, *Energy Environ. Sci.*, 2011, 4, 858-861.
24. X. Rui, Z. Lu, H. Yu, D. Yang, H. H. Hng, T. M. Lim and Q. Yan, *Nanoscale*, 2013, 5, 556-560.
25. Y. Li, J. Yao, E. Uchaker, J. Yang, Y. Huang, M. Zhang and G. Cao, *Adv. Energy Mater.*, 2013, 3, 1171-1175.
26. X. Rui, J. Zhu, W. Liu, H. Tan, D. Sim, C. Xu, H. Zhang, J. Ma, H. H. Hng, T. M. Lim and Q. Yan, *RSC Adv.*, 2011, 1, 117-122.
27. Y. Wang, H. J. Zhang, W. X. Lim, J. Y. Lin and C. C. Wong, *J. Mater. Chem.*, 2011, 21, 2362-2368.
28. S. Wang, S. Li, Y. Sun, X. Feng and C. Chen, *Energy Environ. Sci.*, 2011, 4, 2854-2857.
29. A. Q. Pan, H. B. Wu, L. Zhang and X. W. Lou, *Energy Environ. Sci.*, 2013, 6, 1476-1479.
30. C. Zhang, Z. Chen, Z. Guo and X. W. Lou, *Energy Environ. Sci.*, 2013, 6, 974-978.
31. A.-M. Cao, J.-S. Hu, H.-P. Liang and L.-J. Wan, *Angewandte Chemie International Edition*, 2005, 44, 4391-4395.
32. Y.-S. Hu, X. Liu, J.-O. Müller, R. Schlögl, J. Maier and D. S. Su, *Angew. Chem. Int. Ed.*, 2009, 48, 210-214.
33. X. Chen, H. Zhu, Y.-C. Chen, Y. Shang, A. Cao, L. Hu and G. W. Rubloff, *ACS Nano*, 2012, 6, 7948-7955.
34. K. H. Seng, J. Liu, Z. P. Guo, Z. X. Chen, D. Jia and H. K. Liu, *Electrochem. Commun.*, 2011, 13, 383-386.
35. A. Marschilok, C.-Y. Lee, A. Subramanian, K. J. Takeuchi and E. S. Takeuchi, *Energy Environ. Sci.*, 2011, 4, 2943-2951.
36. J. W. Lee, S. Y. Lim, H. M. Jeong, T. H. Hwang, J. K. Kang and J. W. Choi, *Energy Environ. Sci.*, 2012, 5, 9889-9894.
37. C. Han, M. Yan, L. Mai, X. Tian, L. Xu, X. Xu, Q. An, Y. Zhao, X. Ma and J. Xie, *Nano Energy*, 2013, 2, 916-922.
38. Y. Qian, A. Vu, W. Smyrl and A. Stein, *J. Electrochem. Soc.*, 2012, 159, A1135-A1140.
39. X. Rui, J. Zhu, D. Sim, C. Xu, Y. Zeng, H. H. Hng, T. M. Lim and Q. Yan, *Nanoscale*, 2011, 3, 4752-4758.
40. F. Coustier, J. Hill, B. B. Owens, S. Passerini and W. H. Smyrl, *J. Electrochem. Soc.*, 1999, 146, 1355-1360.
41. H. Yu, X. Rui, H. Tan, J. Chen, X. Huang, C. Xu, W. Liu, D. Y. W. Yu, H. H. Hng, H. E. Hoster and Q. Yan, *Nanoscale*, 2013, 5, 4937-4943.
42. S. Y. Zhan, C. Z. Wang, K. Nikolowski, H. Ehrenberg, G. Chen and Y. J. Wei, *Solid State Ionics*, 2009, 180, 1198-1203.
43. D. M. Yu, S. T. Zhang, D. W. Liu, X. Y. Zhou, S. H. Xie, Q. F. Zhang, Y. Y. Liu and G. Z. Cao, *J. Mater. Chem.*, 2010, 20, 10841-10846.
44. Y. Li, J. Yao, E. Uchaker, M. Zhang, J. Tian, X. Liu and G. Cao, *J. Phys. Chem. C*, 2013, 117, 23507-23514.
45. C.-Y. Lee, A. C. Marschilok, A. Subramanian, K. J. Takeuchi and E. S. Takeuchi, *Phys. Chem. Chem. Phy.*, 2011, 13, 18047-18054.
46. J. P. Pereira-Ramos, R. Messina, L. Znaidi and N. Baffier, *Solid State Ionics*, 1988, 28–30, 886-894.
47. Y. Katayama, Y. Fukuchi and T. Miura, *Electrochem.*, 2003, 71, 1148-1150.
48. A. Wadsley, *Acta Crystallogr.*, 1957, 10, 261-267.
49. L. A. de Picciotto, K. T. Adendorff, D. C. Liles and M. M. Thackeray, *Solid State Ionics*, 1993, 62, 297-307.
50. A. Sakunthala, M. V. Reddy, S. Selvasekarapandian, B. V. R. Chowdari and P. C. Selvin, *J. Phys. Chem. C*, 2010, 114, 8099-8107.
51. A. Pan, J.-G. Zhang, G. Cao, S. Liang, C. Wang, Z. Nie, B. W. Arey, W. Xu, D. Liu, J. Xiao, G. Li and J. Liu, *J. Mater. Chem.*, 2011, 21, 10077-10084.
52. G. Pistoia, M. Pasquali, M. Tocci, R. V. Moshtev and V. Maner, *J. Electrochem. Soc.*, 1985, 132, 281-284.
53. I. D. Raistrick, *Rev. Chim. Mineral.*, 1984, 21, 456-467.
54. S. Jouanneau, A. Le Gal La Salle, A. Verbaere and D. Guyomard, *J. Electrochem. Soc.*, 2005, 152, A1660-A1667.
55. Y. Feng, F. Hou and Y. Li, *J. Power Sources*, 2009, 192, 708-713.
56. M. Dubarry, J. Gaubicher, D. Guyomard, N. Dupré and C. Grey, *Solid State Ionics*, 2009, 180, 1511-1516.
57. A. C. Marschilok, C. P. Schaffer, K. J. Takeuchi and E. S. Takeuchi, *J. Compos. Mater.*, 2013, 47, 41-49.
58. H. Liu, Y. Wang, K. Wang, Y. Wang and H. Zhou, *J. Power Sources*, 2009, 192, 668-673.

59. V. Manev, A. Momchilov, A. Nassalevska, G. Pistoia and M. Pasquali, *J. Power Sources*, 1995, 54, 501-507.
60. G. Yang, G. Wang and W. Hou, *J. Phys. Chem. B*, 2005, 109, 11186-11196.
61. F. Wu, L. Wang, C. Wu and Y. Bai, *Electrochim. Acta*, 2009, 54, 4613-4619.
62. S. H. Choi and Y. C. Kang, *Chem. –Eur. J.*, 2013, 19, 17305-17309.
63. X. Xu, Y.-Z. Luo, L.-Q. Mai, Y.-L. Zhao, Q.-Y. An, L. Xu, F. Hu, L. Zhang and Q.-J. Zhang, *NPG Asia Mater.*, 2012, 4, e20.
64. K. West, B. Zachau-Christiansen, S. Skaarup, Y. Saidi, J. Barker, I. I. Olsen, R. Pynenburg and R. Koksbang, *J. Electrochem. Soc.*, 1996, 143, 820-825.
65. N. Kumagai and A. Yu, *J. Electrochem. Soc.*, 1997, 144, 830-835.
66. A. Yu, N. Kumagai, Z. Liu and J. Y. Lee, *J. Power Sources*, 1998, 74, 117-121.
67. L. Liu, L. Jiao, J. Sun, Y. Zhang, M. Zhao, H. Yuan and Y. Wang, *Electrochim. Acta*, 2008, 53, 7321-7325.
68. C. Q. Feng, L. F. Huang, Z. P. Guo, J. Z. Wang and H. K. Liu, *J. Power Sources*, 2007, 174, 548-551.
69. H. Song, Y. Liu, C. Zhang, C. Liu and G. Cao, *J. Mater. Chem. A*, 2015, 3, 3547-3558.
70. M. Zhao, L. Jiao, H. Yuan, Y. Feng and M. Zhang, *Solid State Ionics*, 2007, 178, 387-391.
71. Y. Feng, Y. Li and F. Hou, *J. Power Sources*, 2009, 187, 224-228.
72. L. Jiao, L. Liu, J. Sun, L. Yang, Y. Zhang, H. Yuan, Y. Wang and X. Zhou, *J. Phys. Chem. C*, 2008, 112, 18249-18254.
73. S. Y. Chew, C. Feng, S. H. Ng, J. Wang, Z. Guo and H. Liu, *J. Electrochem. Soc.*, 2007, 154, A633-A637.
74. G. Armstrong, J. Canales, A. R. Armstrong and P. G. Bruce, *J. Power Sources*, 2008, 178, 723-728.
75. T. A. Chirayil, P. Y. Zavalij and M. S. Whittingham, *J. Electrochem. Soc.*, 1996, 143, L193-L195.
76. B. Zachau-Christiansen, K. West and T. Jacobsen, *Mater. Res. Bull.*, 1985, 20, 485-492.
77. A. M. Kannan and A. Manthiram, *Solid State Ionics*, 2003, 159, 265-271.
78. C. Tsang and A. Manthiram, *J. Electrochem. Soc.*, 1997, 144, 520-524.
79. H. Li, P. He, Y. Wang, E. Hosono and H. Zhou, *J. Mater. Chem.*, 2011, 21, 10999-11009.
80. E. Baudrin, G. Sudant, D. Larcher, B. Dunn and J.-M. Tarascon, *Chem. Mater.*, 2006, 18, 4369-4374.
81. X. Rui, D. Sim, C. Xu, W. Liu, H. Tan, K. Wong, H. H. Hng, T. M. Lim and Q. Yan, *RSC Adv.*, 2012, 2, 1174-1180.
82. Q. Zhao, L. Jiao, W. Peng, H. Gao, J. Yang, Q. Wang, H. Du, L. Li, Z. Qi, Y. Si, Y. Wang and H. Yuan, *J. Power Sources*, 2012, 199, 350-354.
83. D. Chao, C. Zhu, X. Xia, J. Liu, X. Zhang, J. Wang, P. Liang, J. Lin, H. Zhang, Z. X. Shen and H. J. Fan, *Nano Lett.*, 2015, 15, 565-573.
84. M. M. Rahman, J.-Z. Wang, N. H. Idris, Z. Chen and H. Liu, *Electrochim. Acta*, 2010, 56, 693-699.
85. Y. Shi, S.-L. Chou, J.-Z. Wang, H.-J. Li, H.-K. Liu and Y.-P. Wu, *J. Power Sources*, 2013, 244, 684-689.
86. C. Nethravathi, B. Viswanath, J. Michael and M. Rajamath, *Carbon*, 2012, 50, 4839-4846.
87. S. Yang, Y. Gong, Z. Liu, L. Zhan, D. P. Hashim, L. Ma, R. Vajtai and P. M. Ajayan, *Nano Lett.*, 2013, 13, 1596-1601.
88. C. Nethravathi, C. R. Rajamathi, M. Rajamathi, U. K. Gautam, X. Wang, D. Golberg and Y. Bando, *ACS Appl. Mater. Inter.*, 2013, 5, 2708-2714.
89. L. Mai, Q. Wei, Q. An, X. Tian, Y. Zhao, X. Xu, L. Xu, L. Chang and Q. Zhang, *Adv. Mater.*, 2013, 25, 2969-2973.
90. H. Liu, Y. Wang, K. Wang, E. Hosono and H. Zhou, *J. Mater. Chem.*, 2009, 19, 2835-2840.
91. C. Niu, J. Meng, C. Han, K. Zhao, M. Yan and L. Mai, *Nano Lett.*, 2014, 14, 2873-2878.
92. A. Pan, H. B. Wu, L. Yu and X. W. Lou, *Angew. Chem. Int. Ed.*, 2013, 52, 2226-2230.
93. J. Gaubicher, C. Wurm, G. Goward, C. Masquelier and L. Nazar, *Chem. Mater.*, 2000, 12, 3240-3242.
94. S. C. Yin, H. Grondey, P. Strobel, M. Anne and L. F. Nazar, *J. Am. Chem. Soc.*, 2003, 125, 10402-10411.
95. X. H. Rui, N. Ding, J. Liu, C. Li and C. H. Chen, *Electrochim. Acta*, 2010, 55, 2384-2390.
96. P. Fu, Y. Zhao, Y. Dong, X. An and G. Shen, *J. Power Sources*, 2006, 162, 651-657.
97. P. Fu, Y. Zhao, Y. Dong, X. An and G. Shen, *Electrochim. Acta*, 2006, 52, 1003-1008.
98. X. Zhu, Y. Liu, L. Geng, L. Chen, H. Liu and M. Cao, *Solid State Ionics*, 2008, 179, 1679-1682.
99. X. H. Rui, C. Li, J. Liu, T. Cheng and C. H. Chen, *Electrochim. Acta*, 2010, 55, 6761-6767.
100. Q. Chen, J. Wang, Z. Tang, W. He, H. Shao and J. Zhang, *Electrochim. Acta*, 2007, 52, 5251-5257.
101. Y. Li, Z. Zhou, X. Gao and J. Yan, *Electrochim. Acta*, 2007, 52, 4922-4926.
102. C. Chang, J. Xiang, X. Shi, X. Han, L. Yuan and J. Sun, *Electrochim. Acta*, 2008, 54, 623-627.
103. Y. Q. Qiao, J. P. Tu, J. Y. Xiang, X. L. Wang, Y. J. Mai, D. Zhang and W. L. Liu, *Electrochim. Acta*, 2011, 56, 4139-4145.
104. H. Liu, C. Cheng, X. Huang and J. Li, *Electrochim. Acta*, 2010, 55, 8461-8465.
105. Y. N. Ko, H. Y. Koo, J. H. Kim, J. H. Yi, Y. C. Kang and J.-H. Lee, *J. Power Sources*, 2011, 196, 6682-6687.
106. C. Wang, H. Liu and W. Yang, *J. Materials Chemistry*, 2012, 22, 5281-5285.
107. C. Chang, J. Xiang, X. Shi, X. Han, L. Yuan and J. Sun, *Electrochim. Acta*, 2008, 53, 2232-2237.
108. T. Jiang, W. Pan, J. Wang, X. Bie, F. Du, Y. Wei, C. Wang and G. Chen, *Electrochim. Acta*, 2010, 55, 3864-3869.
109. X. H. Rui, C. Li and C. H. Chen, *Electrochim. Acta*, 2009, 54, 3374-3380.
110. X. Rui, D. Sim, K. Wong, J. Zhu, W. Liu, C. Xu, H. Tan, N. Xiao, H. H. Hng, T. M. Lim and Q. Yan, *J. Power Sources*, 2012, 214, 171-177.
111. H. Liu, P. Gao, J. Fang and G. Yang, *Chem. Commun.*, 2011, 47, 9110-9112.
112. L. Zhang, X. L. Wang, J. Y. Xiang, Y. Zhou, S. J. Shi and J. P. Tu, *J. Power Sources*, 2010, 195, 5057-5061.

113. S. Xun, J. Chong, X. Song, G. Liu and V. S. Battaglia, *J. Mater. Chem.*, 2012, 22, 15775-15781.
114. J. Zhai, M. Zhao, D. Wang and Y. Qiao, *J. Alloys Compd.*, 2010, 502, 401-406.
115. Q. Kuang, Y. Zhao, X. An, J. Liu, Y. Dong and L. Chen, *Electrochim. Acta*, 2010, 55, 1575-1581.
116. M. Bini, S. Ferrari, D. Capsoni and V. Massarotti, *Electrochim. Acta*, 2011, 56, 2648-2655.
117. J. S. Huang, L. Yang, K. Y. Liu and Y. F. Tang, *J. Power Sources*, 2010, 195, 5013-5018.
118. M. Ren, Z. Zhou, Y. Li, X. P. Gao and J. Yan, *J. Power Sources*, 2006, 162, 1357-1362.
119. Q. Kuang, Y. Zhao and Z. Liang, *J. Power Sources*, 2011, 196, 10169-10175.
120. C. Sun, S. Rajasekhara, Y. Dong and J. B. Goodenough, *ACS Appl. Mater. Inter.*, 2011, 3, 3772-3776.
121. S. Zhong, L. Liu, J. Liu, J. Wang and J. Yang, *Solid State Commun.*, 2009, 149, 1679-1683.
122. J. Yan, W. Yuan, Z.-Y. Tang, H. Xie, W.-F. Mao and L. Ma, *J. Power Sources*, 2012, 209, 251-256.